Classification of Breast Masses on Contrast-Enhanced Magnetic Resonance Images Through Log Detrended Fluctuation Cumulant-Based Multifractal Analysis

Filipe Soares, Filipe Janela, Manuela Pereira, João Seabra and Mário M. Freire, *Member, IEEE*

***Abstract*—This article proposes a multi-scale automated model for the classification of suspicious malignancy of breast masses, through log detrended fluctuation cumulant-based multifractal analysis of images acquired by dynamic contrast enhanced magnetic resonance. Features for classification are extracted by computing the multifractal scaling exponent for each of the 70 clinical cases and, by quantifying the *log-cumulants* reflecting multifractal information related with texture of the enhanced lesions. The output is compared to the radiologist diagnosis that follows the Breast Imaging - Reporting and Data System (BI-RADS). The results suggest that the *log-cumulant* c_2 can be effective to classify typically biopsy-recommended cases. The performance of a supervised classification was evaluated by receiver operating characteristics (ROC) with an area under the curve of 0.985. The proposed multifractal analysis can contribute to novel feature classification techniques to aid radiologists every time there is a change in clinical course, namely when biopsy should be considered.**

***Index Terms*—Breast Cancer, Computer-aided diagnosis, Dynamic contrast-enhanced, Feature extraction, Magnetic resonance imaging, Multi-scale, Multifractal analysis.**

I. Introduction

MAGNETIC Resonance Imaging (MRI) of the breast has been shown to be the most sensitive modality for scanning high-risk women, offering valuable information about breast conditions that cannot be obtained by other imaging modalities, such as mammography or ultrasound [1]. Dynamic Contrast Enhanced - Magnetic Resonance Imaging (DCE-MRI) techniques are based on the injection of a MRI contrast agent and acquisition of T1-weighted images over time, which provides information on the diffusion of the agent to the tissues.

The diagnosis is generated by visual examination of morphological features and contrast-enhancement kinetics (functional features) using descriptors established in the Breast Imaging - Reporting and Data System (BI-RADS) lexicon [2]. Focus and foci are enhancements measuring less than 5 mm in diameter that are too small to be characterized in MRI. These lesions are typically stable on follow-up, may result from hormonal changes and are considered a part of the normal background enhancement pattern of the breast. Only bigger lesions than foci can be diagnosed and from those, malignant ones tend to present more irregular shape, speculated margins, and heterogeneous inner enhancement [3]. A lesion with contrast-enhancement kinetics of rapid initial rise, followed by a drop-off (washout) in the delayed phase, can have a positive predictive value of 77% for malignancy [4], [5]. Fischer et al. [6] proposed a scoring system (Göttingen score) based on the combination of DCE-MRI morphological and functional features that is coadjuvant in the assessment of the BI-RADS grade. Nevertheless, clinical interpretation of breast MRI still remains largely subjective and the reported findings are often qualitative, having therefore an impact on the accuracy of the diagnosis. Computer aided diagnosis (CADx) arises in this context as an approach to reduce the subjectivity in human interpretation by improving specificity and possibly sensitivity, through a quantitative measurement and by offering the possibility of a reduction of the time needed for the breast MRI analysis [7].

The simplest heuristic model used to distinguish between malignant and benign lesions in DCE-MRI is known as the three-time-points (3TP) [8], [9], where points are selected along the time-intensity sequence during contrast uptake to characterize the enhancement slope and the washout rate. The enhancement pattern in the 3TP method varies according to the imaging protocol, but it allows a pixel-by-pixel kinetic analysis from the intensity values. Combining certain physiological parameters with a mathematical model of the temporal kinetics of the signal, parameter maps can be displayed. These depend on the overall shape of the tissue curves, and thus reflect tissue physiology only indirectly. In

Manuscript received July 30, 2012; revised August 16, 2013; accepted August 17, 2013. This work was partially funded by the Fundação para a Ciência e a Tecnologia through grant SFRH/BDE/15624/2006, by Siemens S.A. Healthcare Sector, by Instituto de Telecomunicações and by University of Beira Interior, Portugal. *Asterisk indicates corresponding author.*

*Filipe Soares is with Siemens S.A. Healthcare Sector, 4456-901 Perafita, Portugal (e-mail: filipecruzsoares@gmail.com).

Filipe Janela and João Seabra are with Siemens S.A. Healthcare Sector, 4456-901 Perafita, Portugal.

Filipe Soares, Manuela Pereira and Mário M. Freire are with Instituto de Telecomunicações, Department of Computer Science, University of Beira Interior, 6201-001 Covilhã, Portugal.

addition, the accuracy of the 3TP method is nearly insensitive to the temporal sampling rate of the acquired data, as shown in [10], which makes it preferable to apply the 3TP on data acquired by standard imaging protocols that suffer from low temporal resolution. Moreover, due to the trade-off between spatial and temporal resolutions, a standard protocol allows the use of morphological and functional analysis in the same data. Albeit providing only an imperfect gold standard which does not necessarily reflect the biological truth, the 3TP represents a clinical routine for visual examination of DCE-MRI data, and hence may serve as a reference model.

Contrast enhancement of findings, extensively used in mammography [11]–[13], aim to increase the contrast over some threshold levels which often require manual adjustments towards the trade-off between noise suppression and detail preservation. To automate lesion classification in MRI, features extracted by computer-based image analysis have been investigated as diagnostic aids, with mathematical descriptors related with those visually used by radiologists [14]. This approach adds capabilities for the analysis of textural, morphological and kinetic enhancement features. Previous studies [15]–[17] were focused on assessing the margin sharpness of the lesions. However, this is only one of the parameters evaluated by the radiologist. A plethora of other algorithms and classifiers have been proposed. The automated interpretation approach based on enhancement variance dynamics was proposed by Chen et al. [18], using linear discriminant analysis for lesion classification after feature extraction. Later in [19], fuzzy c-means clustering was used to identify enhancement kinetics. Yao et al. proposed in [20] a pixel-by-pixel classification method based on texture analysis and wavelet transform for tumor evaluation in breast DCE-MRI. In [21], Zheng et al. used spatiotemporal enhancement pattern and Fourier transform to analyze breast images. Back-propagation neural network classification of segmented regions was proposed by Meinel et al. [22] using shape and kinetic features combined. Artificial neural networks have been one of the most investigated approaches for the classification of breast lesions in DCE-MRI [23]–[26]. However, it has been shown that support vector machine (SVM) lead to a better performance than a variety of other machine learning techniques in the classification of breast lesions [27]–[30]. Moreover, a CADx system should work as a second-look for the radiologist and therefore it should focus on a comprehensive set of characteristics of the lesions, including features that are indistinguishable to the human eye.

Since images of breast tissue are characterized by a high degree of self-similarity [31], i.e., several parts look as the whole image, if structural deviations from the global regularity of the background occur, then they may be considered breast lesions. Those irregularities can be characterized under the light of fractal or multifractal analysis. The fractal theory has been proposed for breast tumors detection and classification [16], [17]. However, in these studies it was used for margin sharpness characterization only and in [17], Penn et al. have shown that nearly two thirds of the cancers were categorized inconclusive in terms of fractal dimension. A potential problem is related with the inability of the fractal dimension to uniquely characterize the texture pattern. Different fractal sets may share the same fractal dimension values and yet have different appearances [32]. Nevertheless, from the point of view of multifractal theory, more advanced approaches do exist allowing a deeper exploration of the potential of this theory for medical image analysis. The multifractal analysis provides a spectrum of fractal dimensions, characterizing multiple irregularities. This can potentially give more information about the image than the single fractal dimension, without being exclusively focused on lesion margins.

A preliminary study from our group [31] on the application of the multifractal analysis to mammographic images showed very promising results in the detection of lesions. There are no further conclusive results of multifractal-based analysis in DCE-MR images of the breast. The multifractal study of mammograms has been done with wavelet-based multifractal theory in [33], using the Wavelet Transform Modulus Maxima (WTMM), a promising method with high precision in the scaling analysis in spite of being complex, especially for high-dimensional objects. In our work, the selected method for the multifractal analysis is the Multifractal Detrended Fluctuation Analysis (MF-DFA) [34], a reliable alternative to WTMM being less sensitive to lack of resolution, which is beneficial given the low spatial resolution of the breast DCE-MRI data. The MF-DFA is based on the Detrended Fluctuation Analysis (DFA) [35], a very efficient method in avoiding spurious detection of artifactual correlations. There are evidences that MF-DFA provides similar results to WTMM but the former is simpler and more accurate for low temporal resolution time series. [36], [37]. In fact, WTMM false multifractality can be even more evidenced in medical images, as verified in the study with mammographic images [31].

In this work, multifractal analysis of breast lesions in DCE-MR images is explored for diagnosis. For the first time, to the best of our knowledge, the MF-DFA is applied in the discrimination of breast lesions in MRI. Our goal is to classify suspicious malignancy of breast masses through a multi-scale automated model that extract self-similarity features by Log Detrended Fluctuation Cumulant-based Multifractal Analysis. These features are studied in order to characterize in detail the morphology and texture of the contrast-enhanced lesions in a supervised classification scheme.

II. Materials and Methods

Existing fractal methods of texture analysis rely on the fractal dimension as a function of scale. We explore the application of multifractal analysis for characterizing multi-scale changes in the textural information related with self-similarity regularity. Multifractal signals are intrinsically more complex than (mono) fractals. Multifractal analysis exploits both local irregularity (roughness) of a given measure and the global distribution of this irregularity, as reported in [31].

A model for multifractal image analysis is proposed as illustrated in Fig. 1. In particular, it comprises a decision-support system in the diagnosis of breast cancer with DCE-MRI. The images and respective clinical reports are the

input of the model. Section II.A and II.B will follow with details on how the images were acquired and characterization of the dataset. Log Detrended Fluctuation Cumulant-Based Multifractal Analysis was implemented in order to evaluate the degree of structural deviation of a tumor from the global regularity of the surrounding breast tissue. The irregularities arise at multiple scales and are characterized through a spectrum of fractal dimensions, the multifractal spectrum, and summarized by *log-cumulants* from the scaling exponent. The core of the multifractal analysis is described in Section II.C and the algorithm for the extraction of features is presented in Section II.D. The 3TP model based on the kinetic curves of enhancement described in Section I was also implemented for comparison with the model proposed herein, using the same acquisition protocol.

A. Image acquisition

Experimental data was acquired using a Siemens Trio 3T MR Scanner at the health institution Clínica João Carlos Costa, Viana do Castelo, Portugal. This study was approved by the research ethics committee of the health institution. Dynamic imaging was performed using a T1-weighted FLASH 3D (FL3D) pulse sequence with fat saturation following subtraction. The patients were scanned in prone position using a standard double breast coil. The acquisition protocol parameters were 3.76 ms of repetition time (TR), 1.38 ms of echo time (TE) with flip angle = 12º, the in-plane spatial resolution was 0.65×0.65 mm^2 and the slice thickness 0.6 mm for the generated 3D volumes. Each slice of the volumes contains 448×448 pixels for a typical field of view of 30×30 cm^2. Imaging is performed before and after a bolus intravenous injection of 0.1 mmol/kg of Gadopentetate dimeglumine (Gd-DTPA). Five bilateral axial acquisition series were taken per patient at intervals of 1 min and 51 s. The first post-contrast images acquired after contrast arrival were used for the multifractal analysis of the enhanced lesions since it was found that the information from the initial portion of the time was the most predictive of malignancy as reported in [25]. The time points 0, 111 s and 444 s were used for 3TP.

B. Dataset characterization and tumor selection

A dataset of 70 clinical cases were sequentially selected retrospectively by a radiologist not including vascular structures, architectural distortions and other non-masses. A diagnosis report was processed with a BI-RADS grade assigned to each case, according to the morphology (see Fig. 2) and dynamic enhancement of the findings. In addition to the BI-RADS grade, the dataset also included the information of biopsy recommendation, which was considered an indication of suspicious malignancy in the present study. The dataset was therefore divided in two main categories of cases: 39 (PM) probably malignant and biopsied – all BI-RADS 4 or 5 plus some BI-RADS 3; 31 (PB) probably benign and non biopsied – all BI-RADS 2 or 3. Simple cases graded with BI-RADS 1 with weak enhancement or nothing to comment on, were not included in the dataset.

After the central slice from the acquired image was defined in the clinical case report, a region of interest (ROI) was selected according to the tumor location to be evaluated, including the background. The sizes of the lesions are evenly distributed among the categories (see Fig. 3). The longest diameter was estimated by the radiologist using an electronic ruler, on the central slice where the lesion was best visualized. Focus and foci findings less than 5 mm were not included since they cannot be specified according to BI-RADS [2].

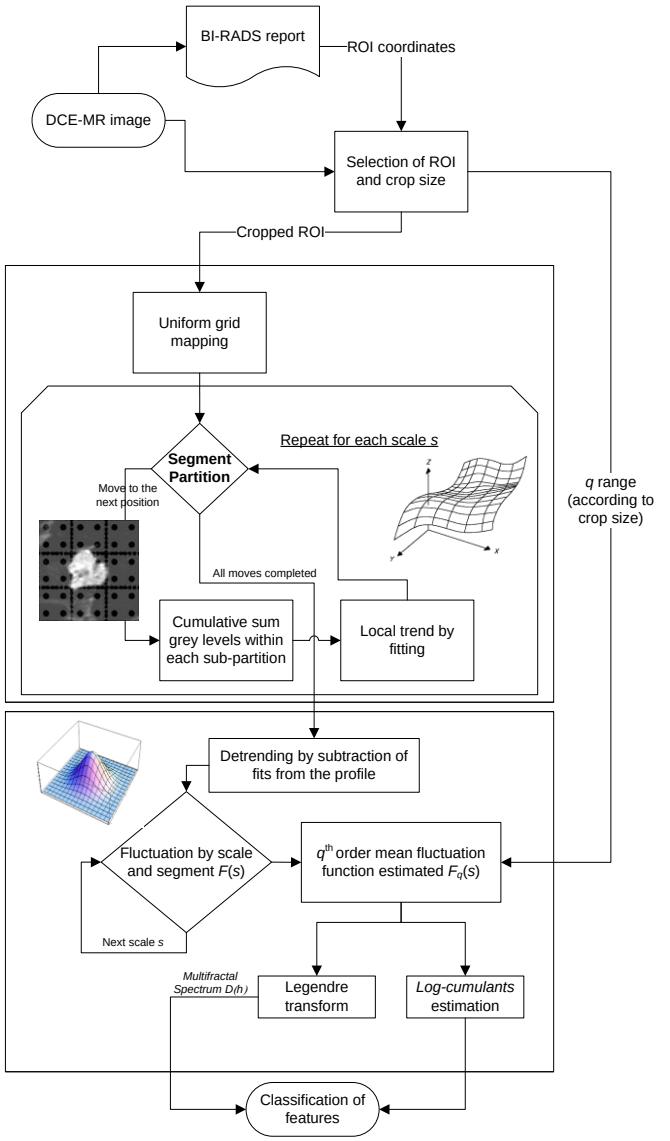

Fig. 1. Flowchart of the model for Log Detrended Fluctuation Cumulant-Based Multifractal Analysis.

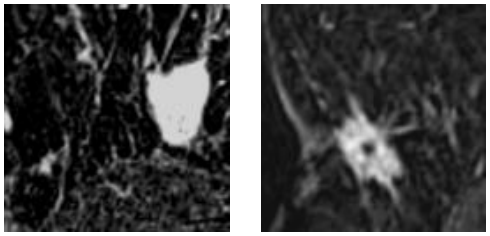

Fig. 2. Morphology features: typical benign case on the left, with oval shaped mass smooth, margin and homogeneous enhancement; typical malignant case on the right with irregular shaped mass, spiculated margin and heterogeneous enhancement.

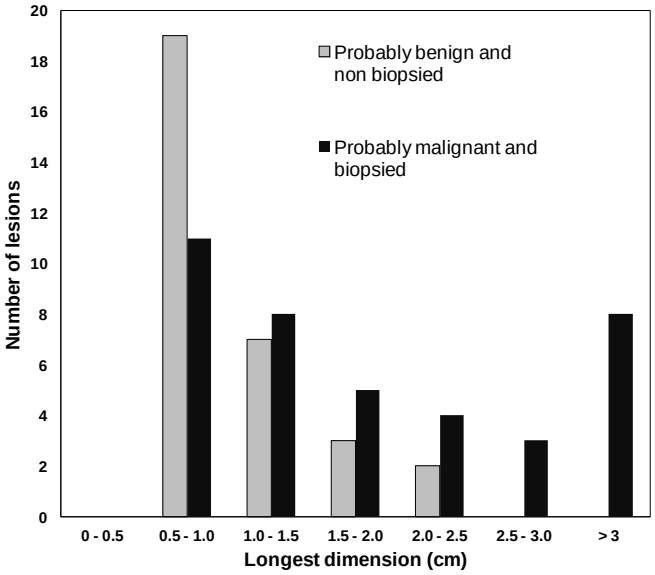

Fig. 3. Histogram of the longest diameter of the lesions in the dataset. The longest diameter was measured where the lesion was best visualized as determined by radiologist.

C. Multifractal analysis

The multifractal spectrum summarizes various degrees of scaling. The dynamics of the scaling can be used as discriminatory descriptors, providing an additional perspective of the data. In this sense, it was attempted to confirm that selected ROIs of the breast MR images have multiple degrees of scaling, by the prevalence of a multifractal spectrum and a non linear multifractal scaling exponent $\tau(q)$. This $\tau(q)$ can be seen as a collection of scaling exponents replacing a single self-similarity parameter and, hence, conveying versatility in actual data analysis.

To interpret breast MR images as multifractals we assume that they are composed of several superimposed sets of fractals. A multifractal object can be characterized by assessing number and size of the fractal sets associated to a certain influence on the scale. These measures are provided by the Hölder exponent h and the Hausdorff dimension $D(h)$, for impact and size, respectively [38]. The relationship between the $D(h)$ and the corresponding h results in the multifractal spectrum. This spectrum describes the quality and quantity of irregularities in the data and its characteristic shape is sensitively dependent on periodic patterns. Therefore, in this study $\tau(q)$ and $D(h)$ were estimated for each tumor images selected.

According to the explanation in the Section I, the selected method for the multifractal study was the Multifractal Detrended Fluctuation Analysis (MF-DFA) [34], due to the limitations in the acquisition of breast MRI data, namely the low spatial resolution. The Detrended Fluctuation Analysis (DFA) presented in [35], comprises an integration of the original data followed by a division into segments of equal length. For each segment, a fitting to the data represents the trend in that segment. A subtraction of a local trend point from a local original point, so-called detrending step, is required to obtain local fluctuations at different timescales. Such procedure enables investigating the scaling properties (self-similarity) and the power-law long-range correlations.

The multifractal generalization of this procedure (MF-DFA) is based on the identification of scaling of the q^{th}-order moments, which have a power-law dependence on the signal length. In this sense, the methodological challenge is how to detect and quantify the scaling and correlation properties with MR images. This method was generalized to be capable of analyzing multifractal properties of objects with higher dimensions by Gu and Zhou in [39]. The MF-DFA two-dimensional method was preliminary applied by Soares et al. in [31] to detect lesions in mammographic studies based on multifractal theory. Following that research work, the MF-DFA adapted here to detect scaling in two-dimensional MR images consists of five stages, where a more detailed description of stage 1 and stage 2 can be found in [39].

Stage 1: Consider a self-similar surface denoted by a two-dimensional array of grey levels $f(i, j)$, where $i = 1, 2, \ldots, M$ and $j = 1, 2, \ldots, N$. The surface is partitioned into $Ms \times Ns$ disjoint segments of lateral size 2^s, as applying a uniform grid map. The scale s is then related with the grid elements size.

Stage 2: In each segment $f_{v,w}$ identified by v and w, the cumulative sum of the grey levels is named $u_{v,w}(i, j)$ where i, j are pixel coordinates and $1 \le i, j \le s$.

Stage 3: The local trend $\tilde{u}$ of the constructed surface $u_{v,w}$ can be determined by fitting it with a polynomial function and the detrended fluctuation function $F(v,w, s)$ are evaluated for each segment as

$$F(v, w, s) = \sqrt{\frac{1}{s^2}\sum_{i=1}^{s}\sum_{j=1}^{s}\left[u_{v,w}(i, j) - \tilde{u}_{v,w}(i, j)\right]^2}, \qquad (1)$$

where many fitting procedures (m-order two-dimensional polynomials) $\tilde{u}$ can be used. Since the detrending is done by the subtraction of the fits from the profile, the order of the polynomials differs in their capability of eliminating trends in the data. Second-order was confirmed to be adequate for spurious free fitting with MRI data detrending, this way eliminating the influence of possible first-order trends in the original two-dimensional array, for scales larger than the segment size. Therefore, the following polynomial is adopted,

$$\tilde{u}_{v,w}(i, j) = ai^2 + bj^2 + cij + di + ej + f, \qquad (2)$$

where $1 \le$ i, j $\le$ s, and a, b, c, d, e, and f are free parameters that can be estimated through matrix operations, derived from the least-squares method.

Stage 4: The q^{th}-order mean fluctuation function is obtained by averaging over all segments lengths s, that is, by [39]:

$$F_q(s) = \left\{\frac{1}{M_s N_s}\sum_{v=1}^{M_s}\sum_{w=1}^{N_s}\left[F(v, w, s)\right]^q\right\}^{\frac{1}{q}}, \qquad (3)$$

where q can take any real value except zero. The parameter q can be seen as a focus control of a "microscope lens" for exploring different regions of irregularity. Several ranges of q were tested leading to an optimal $-18 < q < 18$ range for the problem in study. The key property of $F_q(s)$ is that for an

image with self-similarity properties, a presence of a power-law scaling is revealed with a linear relationship on a double log plot within a significant range of *s*. We are interested in how the fluctuation functions depend on *q* and how this dependence is related to multifractal features of the surface, determining how it depends on scale.

Stage 5: The scaling behavior of the fluctuation function may be determined by varying *s* in the range from 4 to 8 with the scaling relation between the detrended fluctuation function F_q and the size scale *s*, given by [34]:

$$F_q(s) \sim s^{h(q)}, \tag{4}$$

where the $h(q)$ is called generalized Hurst exponent, a family of scaling exponents. This is the final outcome of the MF-DFA, which is a decreasing function of *q* for multifractal surfaces. For monofractals, it remains constant with identical scaling behavior for all values of *q*. The range of the scales aforementioned was chosen following the recommendations in [34] for statistically reliability and in agreement to the procedure of fitting our MR images in stage 3.

In the multifractal analysis $D(h)$, $h(q)$ and $\tau(q)$ may be related resorting to the Legendre transform [40], being *d* the dimension of space (for an image, $d = 2$), as

$$D(h) = \inf_{q \neq 0}(d + qh(q) - \tau(q)). \tag{5}$$

D. Self-similarity extraction

The previous method of multifractal analysis is applied to each clinical case, to obtain a possible non linear scaling exponent $\tau(q)$ and a spectrum $D(h)$ to confirm the presence of multifractality.

Instead of measuring the multifractal scaling exponent $\tau(q)$ theoretically for all *q*, an empirical scaling analysis of $\tau(q)$ has been suggested to be regarded as a polynomial expansion of order *p* [41]:

$$\tau(q) = \sum_{p \geq 1} c_p \frac{q^p}{p!}. \tag{6}$$

The *log-cumulants* c_p that do not depend on scale can be obtained from the scale dependence of $C(j,p)$, the cumulant of order $p \geq 1$ and scale *j*, of a random variable *X*, by [42]:

$$C(j, p) = c^0{}_p + c_p \ln 2^j. \tag{7}$$

A process is said to be multifractal when $\tau(q)$ departs from linear behavior with $c_2 \neq 0$. The most commonly used *Log-normal* multifractal in practice can be characterized only by c_1 and $c_2 \neq 0$, but more complex multifractal models may involve polynomials of order higher than 2. Consequently, the study of $\tau(q)$ can be rephrased in terms of the *log-cumulants* estimated by linear regression in (6).

We want to evaluate if the ROIs from the DCE-MRI of the breast could be represented or not by $p \geq 2$, $c_p \neq 0$ and thus reveal a simple or more complex multifractal behavior. We retain this *log-cumulant* triplet (c_1, c_2, c_3) as features that allow differentiating tumors with the aid of supervised classification.

Our self-similarity extraction, presented in Algorithm 1, calculates (when possible) *log-cumulants* from the estimated scaling exponent, but also descriptors of a spectrum $D(h)$. Different spectral characteristics are quantified (Fig. 4). This quantification of features values should not be confused with the quantification of MR signal intensity. This article does not describe any conversion between MR signal intensity and contrast agent concentration, because values used in the analysis are not meant to be quantitatively comparable between scans. In this study, only the relative intensity between pixels in a ROI (including the background of a lesion) is used to characterize anatomical detail of the contrast-enhanced lesions.

Algorithm 1 Self-similarity extraction

1) For each image *k* in the dataset
   a) Set *q* step according to *k* size
   b) Set *q* range *qr* as $-2 < qr < 2$ in steps of *qstep*
   c) For each moment *q* between *qr*
      i) Compute mean fluctuation function $F_q(s)$ between scales *s*
      ii) Estimate multifractal scaling exponent $\tau(q)$
      iii) Estimate multifractal spectrum $D(h)$ from $F_q(s)$
   d) Compute *log-cumulant* c_1, c_2, c_3 from $\tau(q)$
   e) Compute descriptors *LS*, *H*, *Dh*, *W*, RS, from $D(h)$
   f) Store the multifractal descriptors and *log-cumulants* on a feature matrix $(f(qr),k)$
   g) Expand *q* range and repeat Step b) to Step e) while all members of $f \in \Re$, otherwise jump to next image *k*

2) For each feature $f(qr)$, vary gamma γ and regularization parameter *C*
   a) Classify image *k* into two main categories (PB or PM) with SVM in LOO cross-validation scheme.
   b) Obtain the performance metrics A_z, Sensitivity, Specificity, Accuracy, according to the actual clinical diagnosis of *k*
   c) Store a matrix of performance metrics for each combination of SVM parameters per feature

3) Select the profile of SVM parameters that maximize A_z as well as Accuracy, for each feature *f* among all *qr*

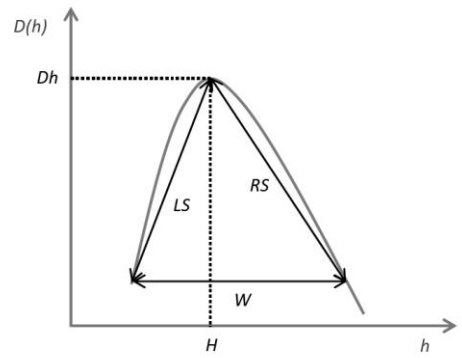

Fig. 4. Scheme of the descriptors used for the multifractal spectrum characterization.

One important descriptor is the *h* where the spectrum is maximum. It shows at which Hölder exponents is positioned the most statistically significant part of the image, i.e. the subsets with maximum fractal dimension. *Hurst* parameter (*H*) is often associated with this exponent reminding the monofractal theory where there is only one fractal dimension.

The corresponding maximum fractal dimension is given by *Dh*. This is directly related with the irregularity of the analysed object. Other important descriptors are the left slope of the curve (*LS*), right slope of the curve (*RS*) and the curve width (*W*). These can be related to how far from monofractal a ROI is.

Supervised classification of tumors was performed by applying SVMs with the extracted multifractal-based features, using the SVM^{light} [43] package for its efficient optimization algorithm, which allows choosing multiple kernel functions to obtain a different classification hyperplane. Radial Basis Function that requires the parameter gamma γ was the kernel used in this work, tested in numerous applications and introduced in a previews study with breast DCE-MRI by Levman et al. [44]. The condition for optimal hyperplane also includes a regularization parameter *C* that controls the trade-off between maximization of the margin and minimization of the training error. Small *C* tends to emphasize the margin while ignoring the outliers in the training data, while large *C* may tend to over fit the training data which is not recommended.

The role of multifractal descriptors and *log-cumulants* is still an open problem for the characterization of tumors. In Algorithm 1, a single feature independent classification was adopted to better understand differences among these features of distinct theoretical meaning. However, for comparison purposes and to evaluate whether joint features may yield better classification, optimized feature sets were also selected among the extracted features based on a ranking criterion using the recursive feature elimination (RFE) [45] combined with SVM. This algorithm determines the feature ranking based on sequential backward elimination that removes one feature at a time, and searches for a nonlinear separating margin to obtain the optimal hyperplane in the feature space.

To select the potentially optimal model for our classification problem (type of kernel function to use, its associated parameters, and *C)*, we applied Leave-one-out (LOO) cross-validation to the working dataset [43]. This LOO technique involves training the machine learning algorithm for estimating the likelihood of malignancy from all cases but one, testing classification on that single case. This procedure is repeated until each case has been tested individually. The cross-validation ensures that all elements of the dataset may be used for both training and testing. Our approach to achieve the best classification based on each feature was to choose the parameters of SVM that produce the model with smaller errors in the cross-validation and use it for testing in order to maximize the accuracy.

The performance of the features in the classification between PM and PB lesions was evaluated by the receiver operating characteristics (ROC) area under the curve (A_z), Sensitivity, Specificity and Accuracy. In order to more accurately place the proposed Log Detrended Fluctuation Cumulant-Based Multifractal Analysis in the landscape of lesion classification in DCE-MRI, the 3TP model was compared by ROC within the same experimental setup.

III. Results

For the images in the dataset, the scaling exponent $\tau(q)$ in Fig. 6 has a concave shape that hence departs from the linear behavior *qH*, known as the signature of self-similarity. Even though, monofractal behaviors occur at some scales (see Fig. 5), particularly for negative moments *q*. In addition, through the estimation of *log-cumulants* it is confirmed in Fig. 7 that c_1 and $c_2 \neq 0$, i.e, we are in the presence of a multifractal process. The concavity of $\tau(q)$ implies $c_2 < 0$. Also, the multifractal spectra $D(h)$ of the analyzed images points to multifractality as they are not limited to a single Hölder exponent *h*.

Solely based on $D(h)$ or $\tau(q)$ (Fig. 6), the distinction between benign and malignant tumors remains unclear. Neither isolated spectral descriptors nor *log-cumulants* were able to properly differentiate the cases. False negatives arise as represented by the outliers in Fig. 7. The outliers from the top report to masses with strong enhancement and all morphological characteristics of malignant findings, as opposed to the relatively slow enhancement of the bottom outliers. In addition, between box-plots from PB and PM there are no statistically significant differences (confidence interval of 95%) and supervised learning classification was conducted.

Fig. 8 and Table I present the performance of the proposed method evaluated by the area under the ROC curve for a SVM classification using each feature derived from multifractal theory, and the top feature set of *RFE-3* features (*LS*, c_2, c_3) identified with the highest accuracy among the features sets.

The *log-cumulant* c_2 appears as the best feature with 0.985 of A_z. This is more effective in classifying typically biopsy-recommended cases, compared with the 3TP model. ROC curves were compared using the Mann–Whitney U-statistics (DeLong et al. [46]). Statistically significant differences were found (p-value < 0.05) between: *c2 vs.* all the others, *3TP vs.* all the others except *c3 and RFE-3*, *c1 vs. c3*, *c1 vs. Dh*.

As it was pointed in Algorithm 1.3), a profile of SVM parameters was optimized (final parameters in Table I) to reach the best A_z and Accuracy. Concurrently, it was evaluated the impact of the q range chosen into the computational efficiency by CPU time in seconds (s). The performance of the best feature *log-cumulant* c_2 is presented in Fig. 9. The optimal classification power was achieved with $-18 < q < 18$ for the problem in study. For larger expansions of q the CPU time starts increasing rapidly. The average execution time per case of the entire Log Detrended Fluctuation Cumulant-Based Multifractal Analysis is 1.65s, on a 2.53GHz Intel® Core™ i5 M540 workstation.

IV. Discussion

In DCE-MRI of the breast, the evaluation of time course kinetics introduces a completely independent parameter that can help to distinguish benign lesions from apparently circumscribed malignant lesions. If a lesion looks benign in terms of morphology, a different diagnosis may be done if signal intensity time courses are evaluated [47]. However, the false-positive rate in MRI is still high and further features which characterize in more detail the morphology and texture

of the contrast-enhanced lesions might be beneficial in the diagnosis of a breast cancer.

Multifractal analysis focuses on understanding and exploring the nature of the irregularities in the image and, not on a single most prevalent irregularity or global trend. The ROI of the enhanced lesions revealed multiple degrees of scaling, i.e., the prevalence of a multifractal spectrum.

Self-similarity features were automatically generated for each early post-contrast images acquired. For each clinical case, the association of extracted multifractal descriptors from *D(h)* and *log-cumulants* from *τ(q)* with BI-RADS visual descriptors was explored. For these computer-extracted features to be accepted, the correlation with morphological descriptors defined in BI-RADS lexicon needs to be established.

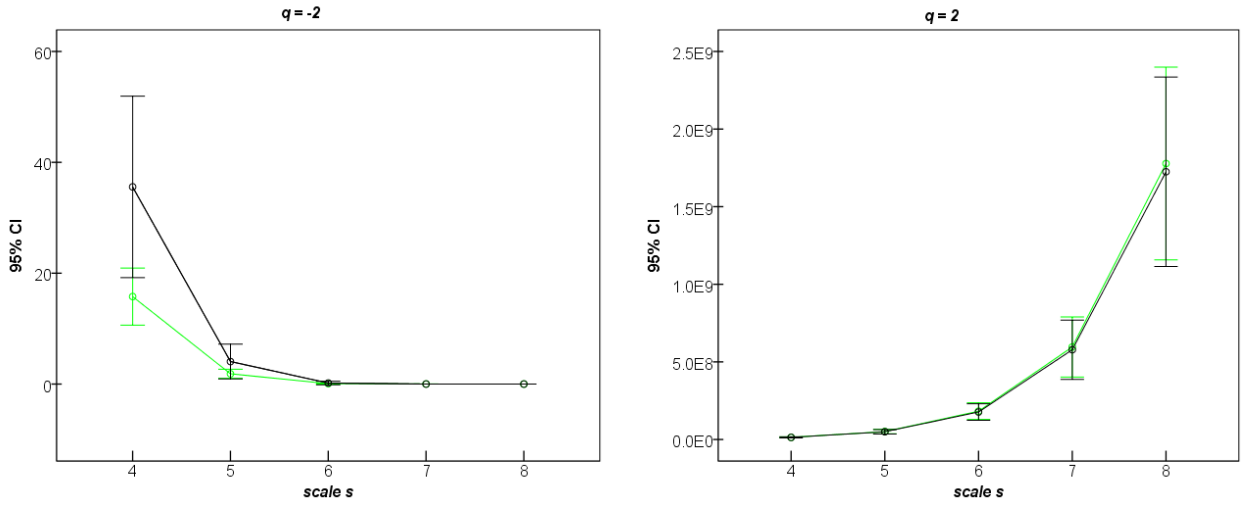

Fig. 5. Detrended fluctuation function *Fq(s)* at different scales for q = -2 (left) and q = 2 (right). PM cases: in black. PB cases: in green. It is shown the presence of scaling range in particular for negative moment q, with the extreme scales showing more deviation from the power law scaling (smaller scales in q = -2 and larger scales in q = 2). Bars from the group of cases represent 95% confidence interval for mean.

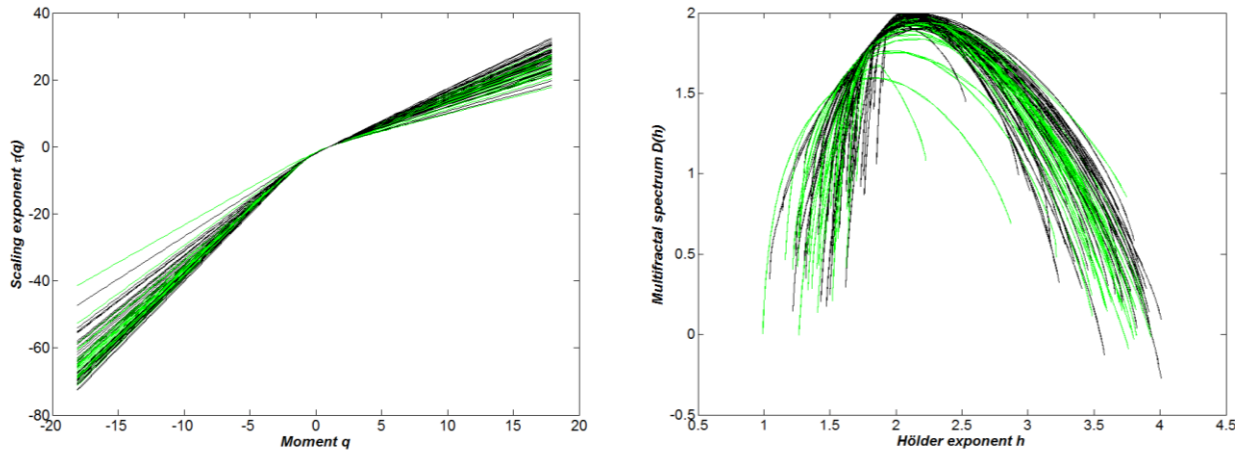

Fig. 6. Estimated scaling exponent *τ(q)* (left) and multifractal spectrum *D(h)* (right) for the lesions in the dataset. PM cases: in black. PB cases: in green.

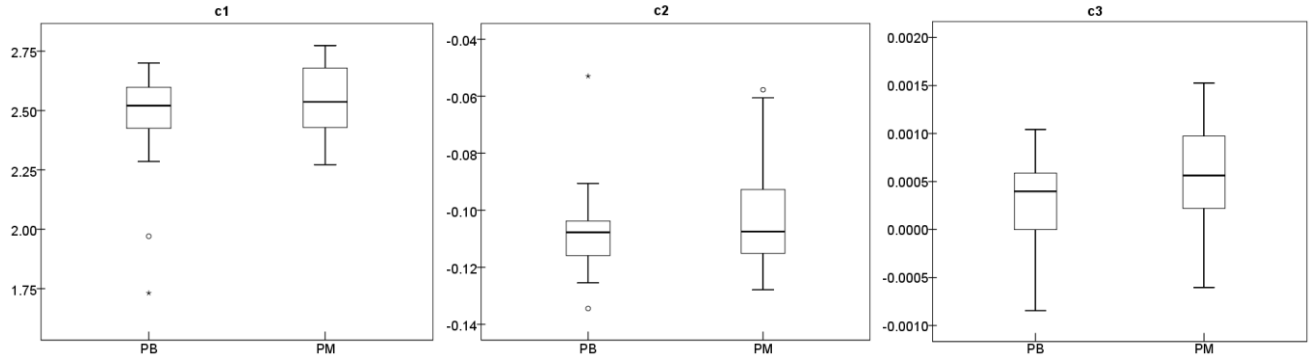

Fig. 7. Comparison of the three *log-cumulants* estimated from *τ(q)* before SVM analysis for PB (left bar) and PM (right bar) cases. The box-plots show the lower and upper quartile and median.

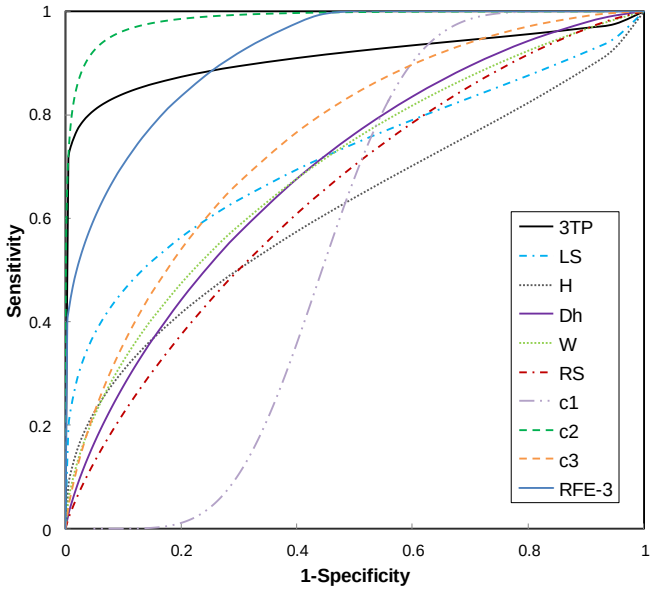

Fig. 8. Comparison of the ROC curves using SVM with the self-similarity extracted features, RFE-3 feature set and the 3TP.

TABLE I
COMPARISON OF THE AREA UNDER THE ROC CURVE A_z AND CORRESPONDING STANDARD DEVIATION (STD) USING SVM

Feature	A_z	(± std)	Sensitivity	Specificity	Accuracy	γ	C
3TP	0.912	0.05	80%	96%	88%		
LS	0.714	0.06	52%	85%	68%	6	10
H	0.617	0.07	42%	80%	61%	6	1
Dh	0.692	0.06	68%	60%	64%	6	100
W	0.695	0.06	59%	70%	64%	6	10
RS	0.646	0.06	61%	60%	60%	3	100
c1	0.555	0.07	94%	37%	65%	2	10
c2	0.985	0.02	94%	94%	94%	3	100
c3	0.753	0.06	67%	70%	68%	6	1000
RFE-3	0.917	0.05	82%	82%	82%	6	100

Gamma γ and regularization parameter (C) as SVM associated kernel parameters.

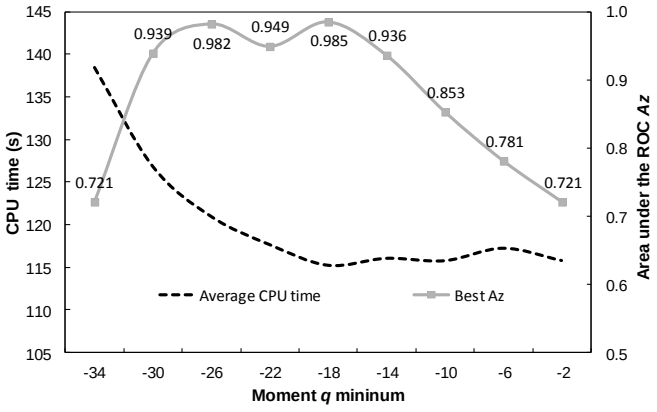

Fig. 9. Comparison of computational efficiency by CPU time in seconds (s) with achieved area under the ROC curve A_z with *log-cumulant* c_2, for multiple expansions of moment q range. The CPU time presented is an average of the total time for running the complete dataset of 70 cases.

It was found that H was related with the most prevalent irregularity of the mass in the ROI, namely shape and margins. *LS* was found to be related with the inner enhancement of the lesion, and how diverged from the monofractal the *D(h)* was, at positive moments q. The *log-cumulants* are known to be related with the aforementioned descriptors of *D(h)*, with c_1 being related with the location of the H, while c_2 with its width W, and c_3 possibly characterizing the asymmetry of *D(h)*. The best result was obtained with *log-cumulant* c_2 that clearly leads us to describe the data as a multifractal rather than monofractal process. This *log-cumulant* represents a compound of the global nature of the multifractal spectrum. In a general interpretation, the malignant cases are more globally inhomogeneous, show higher contrast-enhanced changes that are anti-persistent, and lower contrast-enhanced changes with persistence.

A feature selection algorithm was used as pre-processing for optimization of the hyperdimensional feature space. The rationale of the ranking is that the inputs which are more weighted have the greatest influence on the classification decision. The procedure identified an optimized feature set of three features *RFE-3* (*LS, c2, c3*), but with lower area under the ROC than c_2.

It was empirically found that adjusting *qstep* according to the sizes of the crops would improve the results, because bigger lesions that required larger crop sizes will have more steps in the scaling behavior and, therefore, the steps in *qr* should also be adjusted in the same ratio.

From the observed *Fq(s)* at different scales, positive moments q have similar deviations among PM and PB. Compared with what happens at negative q, with PB deviating less from monofractal than PM at smaller scales, *RS* gave unexpected poor results. Therefore, it should be interesting to deepen the research of *RS* probably with volumetric lesion analysis, since the performance is likely to improve when one takes full advantage of the 3D nature of the data onto the multifractal analysis.

In this study, there were no temporal features associated with the proposed multifractal method, since that would require good temporal sampling rate and standard protocols in DCE-MRI of the breast are limited with respect to temporal resolution (usually 5 time points are found as herein) because it depends on contrast agent circulation time and on MR sequence repetition time. Also for this reason, the results were compared with 3TP instead of more advanced pharmacokinetic models. The latter would require acquisition protocols of higher temporal resolution in order to surpass the diagnosis accuracy of 3TP [10].

Future work would include optimization of different acquisition protocols, with sufficient temporal resolution to extend the multifractal methods in the temporal dimension, and would be compared with the application of more advanced pharmacokinetic models. However, it is worth noticing that the multifractal temporal features derived should not have a correspondence to the pharmacokinetic parameters, which more directly reflect the physiology.

V. Conclusion

In this study, a model for multifractal image analysis, relying on Log Detrended Fluctuation Cumulants, is proposed to assist the radiologist in the diagnosis of breast cancer. According to the results on experimental data from clinical cases of DCE-MRI, the decision-support system presents high accuracy (94%) distinguishing biopsy-recommended lesions from probably benign lesions, with one of the eight features studied. The performance of a supervised classification was evaluated by ROC analysis yielding a maximum area under the curve of 0.985. Even without using all of the consecutive acquired images to build a kinetic curve of enhancement, the best outcome of the proposed model confirms the biopsy recommendations, and overcomes the performance of 3TP, which is a clinical standard protocol for the examination of DCE-MRI data.

References

[1] L. Moy, K. Elias, V. Patel, J. Lee, J. Babb, H. Toth, and C. Mercado, "Is breast MRI helpful in the evaluation of inconclusive mammographic findings?," *American Journal of Roentgenology*, vol. 193, no. 4, p. 986, Oct. 2009.

[2] E. A. Morris, "Illustrated breast MR lexicon," *Semin Roentgenol*, vol. 36, no. 3, pp. 238–249, Jul. 2001.

[3] E. Rosen, S. Smith-Foley, W. DeMartini, P. Eby, S. Peacock, and C. Lehman, "BI-RADS MRI enhancement characteristics of ductal carcinoma in situ," *Breast Journal*, vol. 13, no. 6, p. 545, Nov. 2007.

[4] B. Erguvan-Dogan, G. Whitman, A. Kushwaha, M. Phelps, and P. Dempsey, "BI-RADS-MRI: A Primer," *American Journal of Roentgenology*, vol. 187, no. 2, p. W152, Aug. 2006.

[5] S. A. Jansen, X. Fan, G. S. Karczmar, H. Abe, R. A. Schmidt, M. Giger, and G. M. Newstead, "DCEMRI of breast lesions: Is kinetic analysis equally effective for both mass and nonmass-like enhancement?," *Medical Physics*, vol. 35, no. 7, pp. 3102–3109, Jul. 2008.

[6] U. Fischer, L. Kopka, and E. Grabbe, "Breast Carcinoma: Effect of Preoperative Contrast-enhanced MR Imaging on the Therapeutic Approach1," *Radiology*, vol. 213, no. 3, pp. 881 –888, Dec. 1999.

[7] Y. Gal, A. Mehnert, A. Bradley, D. Kennedy, and S. Crozier, "Feature and Classifier Selection for Automatic Classification of Lesions in Dynamic Contrast-Enhanced MRI of the breast," in *Proceedings of the Digital Image Computing: Techniques and Applications*, 2009, pp. 132–139.

[8] C. Kuhl, P. Mielcareck, S. Klaschik, C. Leutner, E. Wardelmann, J. Gieseke, and H. H. Schild, "Dynamic Breast MR Imaging: Are Signal Intensity Time Course Data Useful for Differential Diagnosis of Enhancing Lesions?1," *Radiology*, vol. 211, no. 1, pp. 101–110, Apr. 1999.

[9] E. Furman-Haran, D. Grobgeld, R. Margalit, and H. Degani, "Response of MCF7 human breast cancer to tamoxifen: evaluation by the three-time-point, contrast-enhanced magnetic resonance imaging method.," *Clinical Cancer Research*, vol. 4, no. 10, pp. 2299 –2304, Oct. 1998.

[10] J. U. Fluckiger, M. C. Schabel, and E. V. R. DiBella, "The effect of temporal sampling on quantitative pharmacokinetic and three-time-point analysis of breast DCE-MRI," *Magnetic Resonance Imaging*, vol. 30, no. 7, pp. 934–943, Sep. 2012.

[11] Y. Zhou, K. Panetta, and S. Agaian, "Mammogram enhancement using alpha weighted quadratic filter," in *Proceedings of the 31st Annual International Conference of the IEEE Engineering in Medicine and Biology Society*, 2009, pp. 3681–3684.

[12] Y. Zhou, K. Panetta, and S. Agaian, "Human visual system based mammogram enhancement and analysis," in *Proceedings of the International Conference on Image Processing Theory Tools and Applications*, 2010, pp. 229–234.

[13] K. Panetta, Y. Zhou, S. Agaian, and H. Jia, "Nonlinear unsharp masking for mammogram enhancement," *Information Technology in Biomedicine, IEEE Transactions on*, vol. 15, no. 6, pp. 918–928, 2011.

[14] M. Giger, "Computerized analysis of images in the detection and diagnosis of breast cancer," *Seminars in Ultrasound CT and MRI*, vol. 25, no. 5, pp. 411–418, Oct. 2004.

[15] K. G. Gilhuijs, M. L. Giger, and U. Bick, "Computerized analysis of breast lesions in three dimensions using dynamic magnetic-resonance imaging," *Medical Physics*, vol. 25, no. 9, pp. 1647–1654, Sep. 1998.

[16] A. I. Penn, L. Bolinger, M. D. Schnall, and M. H. Loew, "Discrimination of MR images of breast masses with fractal-interpolation function models," *Academic Radiology*, vol. 6, no. 3, pp. 156–163, Mar. 1999.

[17] A. Penn, S. Thompson, M. Schnall, M. Loew, and L. Bolinger, "Fractal discrimination of MRI breast masses using multiple segmentations," in *Proceedings of SPIE*, 2000, vol. 3979, pp. 959–966.

[18] W. Chen, M. Giger, L. Lan, and U. Bick, "Computerized interpretation of breast MRI: Investigation of enhancement-variance dynamics," *Medical Physics*, vol. 31, no. 5, p. 1076, Apr. 2004.

[19] W. Chen, M. L. Giger, U. Bick, and G. M. Newstead, "Automatic identification and classification of characteristic kinetic curves of breast lesions on DCE-MRI," *Medical Physics*, vol. 33, no. 8, pp. 2878–2887, Aug. 2006.

[20] J. Yao, J. Chen, and C. Chow, "Breast Tumor Analysis in Dynamic Contrast Enhanced MRI Using Texture Features and Wavelet Transform," *IEEE Journal of Selected Topics in Signal Processing*, vol. 3, no. 1, pp. 94–100, Feb. 2009.

[21] Y. Zheng, S. Englander, S. Baloch, E. Zacharaki, Y. Fan, M. Schnall, and D. Shen, "STEP: Spatiotemporal enhancement pattern for MR-based breast tumor diagnosis," *Medical physics*, vol. 36, no. 7, pp. 3192–3204, Jul. 2009.

[22] L. A. Meinel, A. H. Stolpen, K. S. Berbaum, L. L. Fajardo, and J. M. Reinhardt, "Breast MRI lesion classification: improved performance of human readers with a backpropagation neural network computer-aided diagnosis (CAD) system," *J Magn Reson Imaging*, vol. 25, no. 1, pp. 89–95, Jan. 2007.

[23] R. Lucht, M. Knopp, and G. Brix, "Classification of signal-time curves from dynamic MR mammography by neural networks," *Magnetic Resonance Imaging*, vol. 19, no. 1, pp. 51–57, Jan. 2001.

[24] T. Twellmann, O. Lichte, and T. W. Nattkemper, "An adaptive tissue characterization network for model-free visualization of dynamic contrast-enhanced magnetic resonance image data," *IEEE Transactions on Medical Imaging*, vol. 24, no. 10, pp. 1256–1266, Oct. 2005.

[25] K. Nie, J.-H. Chen, H. J. Yu, Y. Chu, O. Nalcioglu, and M.-Y. Su, "Quantitative Analysis of Lesion Morphology and Texture Features for Diagnostic Prediction in Breast MRI," *Acad Radiol*, vol. 15, no. 12, pp. 1513–1525, Dec. 2008.

[26] C. McLaren, W. Chen, K. Nie, and M. Su, "Prediction of Malignant Breast Lesions from MRI Features: A Comparison of Artificial Neural Network and Logistic Regression Techniques," *Academic radiology*, vol. 16, no. 7, pp. 842–851, Jul. 2009.

[27] T. W. Nattkemper, B. Arnrich, O. Lichte, W. Timm, A. Degenhard, L. Pointon, C. Hayes, and M. O. Leach, "Evaluation of radiological features for breast tumour classification in clinical screening with machine learning methods," *Artif Intell Med*, vol. 34, no. 2, pp. 129–139, Jun. 2005.

[28] J. Levman, T. Leung, P. Causer, D. Plewes, and A. L. Martel, "Classification of Dynamic Contrast-Enhanced Magnetic Resonance Breast Lesions by Support Vector Machines," *IEEE Trans. Med. Imaging*, vol. 27, no. 5, pp. 688–696, May 2008.

[29] A. Basavanhally, S. Doyle, and A. Madabhushi, "Predicting classifier performance with a small training set: Applications to computer-aided diagnosis and prognosis," in *Proceedings of the IEEE International Symposium on Biomedical Imaging: From Nano to Macro*, 2010, pp. 229–232.

[30] S. H. Lee, J. H. Kim, N. Cho, J. S. Park, Z. Yang, Y. S. Jung, and W. K. Moon, "Multilevel analysis of spatiotemporal association features for differentiation of tumor enhancement patterns in breast DCE-MRI," *Med Phys*, vol. 37, no. 8, pp. 3940–3956, Aug. 2010.

[31] F. Soares, M. M. Freire, M. Pereira, F. Janela, and J. Seabra, "Towards the detection of microcalcifications on mammograms through Multifractal Detrended Fluctuation Analysis," in *Proceedings of the IEEE Pacific Rim Conference on Communications, Computers and Signal Processing*, 2009, pp. 677–681.

[32] Q. Guo, J. Shao, and V. Ruiz, "Characterization and classification of tumor lesions using computerized fractal-based texture analysis and support vector machines in digital mammograms," *International Journal*

of Computer Assisted Radiology and Surgery, vol. 4, no. 1, pp. 11–25, 2009.

[33] P. Kestener, J. M. Lina, P. Saint-Jean, and A. Arneodo, "Wavelet-based multifractal formalism to assist in diagnosis in digitized mammograms," *Image Anal Stereol*, vol. 20, no. 3, pp. 169–174, 2001.

[34] J. W. Kantelhardt, S. A. Zschiegner, E. Koscielny-Bunde, S. Havlin, A. Bunde, and H. E. Stanley, "Multifractal detrended fluctuation analysis of nonstationary time series," *Physica A: Statistical Mechanics and its Applications*, vol. 316, no. 1–4, pp. 87–114, Dec. 2002.

[35] C.-K. Peng, S. V. Buldyrev, S. Havlin, M. Simons, H. E. Stanley, and A. L. Goldberger, "Mosaic organization of DNA nucleotides," *Physical Review E*, vol. 49, no. 2, p. 1685, Feb. 1994.

[36] P. Oświecimka, J. Kwapień, and S. Drożdż, "Wavelet versus detrended fluctuation analysis of multifractal structures," *Physical Review E*, vol. 74, no. 1, Jul. 2006.

[37] F. Soares, I. Sousa, F. Janela, J. Seabra, M. Pereira, and M. M. Freire, "Multifractal analysis of Arterial Spin Labeling functional Magnetic Resonance Imaging of the brain," in *Proceedings of the IEEE International Workshop on Medical Measurements and Applications*, 2010, pp. 161–164.

[38] R. Lopes and N. Betrouni, "Fractal and multifractal analysis: A review," *Medical Image Analysis*, vol. 13, no. 4, pp. 634–649, Aug. 2009.

[39] G.-F. Gu and W.-X. Zhou, "Detrended fluctuation analysis for fractals and multifractals in higher dimensions," *Physical Review E*, vol. 74, no. 6, p. 061104, Dec. 2006.

[40] H.-O. Peitgen, H. Jürgens, and D. Saupe, *Chaos and Fractals: New Frontiers of Science*. Springer, 1993.

[41] J. Delour, J. F. Muzy, and A. Arnéodo, "Intermittency of 1D velocity spatial profiles in turbulence: a magnitude cumulant analysis," *Eur. Phys. J. B*, vol. 23, no. 2, pp. 243–248, Sep. 2001.

[42] H. Wendt, P. Abry, and S. Jaffard, "Bootstrap for empirical multifractal analysis," *IEEE Signal Processing Magazine*, vol. 24, no. 4, pp. 38–48, 2007.

[43] T. Joachims, *Making large-scale SVM learning practical*. MIT press, 1999.

[44] J. Levman and A. Martel, "Computer-aided diagnosis of breast cancer from magnetic resonance imaging examinations by custom radial basis function vector machine," in *Proceedings of the 32nd Annual International Conference of the IEEE Engineering in Medicine and Biology Society*, 2010, pp. 5577–5580.

[45] I. Guyon, J. Weston, S. Barnhill, and V. Vapnik, "Gene Selection for Cancer Classification using Support Vector Machines," *Machine Learning*, vol. 46, no. 1–3, pp. 389–422, Jan. 2002.

[46] E. R. DeLong, D. M. DeLong, and D. L. Clarke-Pearson, "Comparing the areas under two or more correlated receiver operating characteristic curves: a nonparametric approach," *Biometrics*, pp. 837–845, 1988.

[47] C. Kuhl and H. Schild, "Dynamic image interpretation of MRI of the breast," *Journal of Magnetic Resonance Imaging*, vol. 12, no. 6, pp. 965–974, Dec. 2000.